ELSEVIER

Chemical Engineering Journal 130 (2007) 75–78

Chemical Engineering Journal

www.elsevier.com/locate/cej

Imaging large vessels using cosmic-ray muon energy-loss techniques

P.M. Jenneson [a,*], W.B. Gilboy [a], S.J.R. Simons [b], S.J. Stanley [c], D. Rhodes [c]

[a] *Department of Physics, University of Surrey, Guildford, Surrey GU2 7XH, UK*
[b] *Department of Chemical Engineering, University College London, Torrington Place, London WC1E 7JE, UK*
[c] *British Nuclear Fuels plc, Research and Technology, Sellafield, Seascale CA20 1PG, UK*

Abstract

Imaging the internal structure of large vessels (2–20 m in diameter) is not possible with most traditional imaging methods. The sheer size renders gamma-ray and other high-energy photon, neutron, electrical and acoustic techniques useless, whilst the use of high-energy accelerators required to produce charged-particles of sufficient energy are impractical in most industrial situations. The use of naturally occurring high-energy (∼GeV) cosmic-ray mu-mesons (muons) provides an effective solution to the penetration problem. The problems of low intensity at near-horizontal angles with the cosmic-ray muon flux are addressed by using energy-loss imaging methods. In other methodologies, using charge-particle energy-loss imaging techniques, only a few events are needed compared to many thousands required if attenuation measurements were to be employed. The energies of horizontal cosmic-ray muons are distributed largely between 0.1 and 1000 GeV with a mean energy of about 50 GeV. Radiation Transport Monte-Carlo methods (GEANT4) have been used to calculate the energy loss for a selection of industrial materials in the energy range of interest. The energy loss of the muons along a ray-sum are modelled and compared to attenuation losses along the ray-sum using energy resolving detectors in coincidence before and after the sample. The energy-loss spectra across different samples are measured, demonstrating that embedded materials can be identified with as few as 10 muons passing through the sample. It is proposed that the imaging modality can be extended into a full tomographic modality allowing material identification within each voxel.

Keywords: Cosmic-ray; Muons; Monte-Carlo methods

1. Cosmic-ray radiation

Primary cosmic-rays consist mainly of particles, such as protons, alpha particles and occasionally heavier particles that are accelerated through space to energies in excess of many TeV. Each primary cosmic-ray particle results in the formation of a shower of thousands of secondary cosmic-rays. At sea level, this shower is around a kilometre in diameter and 1 m thick. The primary components of the secondary cosmic radiation shower at sea level are muons, electrons, neutrons and gamma-rays [1]. Pions are unstable particles with a short lifetime of 26 ns, and are not observed very frequently at sea level. Muons, however, have a longer lifetime of 2.2 μs. Consequently, due to relativistic time dilation, the muon flux at sea level is approximately 160 particles per second per square metre. A muon is essentially a "heavy electron" with a mass of $207m_e$, where m_e is the rest mass of the electron [2]. The muon also carries a single negative or positive charge. The variation in intensity of the muon flux with respect to zenith angle is commonly thought of as a $\cos^2\theta$ distribution. This implies zero flux at the horizontal angle, but there is actually a measurable flux of muons at this angle [3]. The energy distribution of these muons is shown in Fig. 1.

2. Mu-meson interactions

High-energy muons lose energy in several ways as they pass through matter. The mean energy loss per unit path length over a small length (the stopping power) can be expressed as the sum of four different processes, see Eq. (1).

$$\left.\frac{\mathrm{d}E}{\mathrm{d}x}\right]_{\text{Total}} = \left.\frac{\mathrm{d}E}{\mathrm{d}x}\right]_{\text{Ionisation}} + \left.\frac{\mathrm{d}E}{\mathrm{d}x}\right]_{\text{Bremsstrahlung}} + \left.\frac{\mathrm{d}E}{\mathrm{d}x}\right]_{\text{Pair-production}} + \left.\frac{\mathrm{d}E}{\mathrm{d}x}\right]_{\text{Nuclear-interaction}} \quad (1)$$

The main process by which energy is lost is due to ionisation (although other interactions make small contributions). The Bethe–Bloch expression for stopping power can be used to calculate the continuous energy loss due to ionisation [4],

* Corresponding author. Tel.: +44 1483 689419; fax: +44 1483 686781.
E-mail address: p.jenneson@surrey.ac.uk (P.M. Jenneson).

1385-8947/$ – see front matter © 2006 Elsevier B.V. All rights reserved.
doi:10.1016/j.cej.2006.06.016

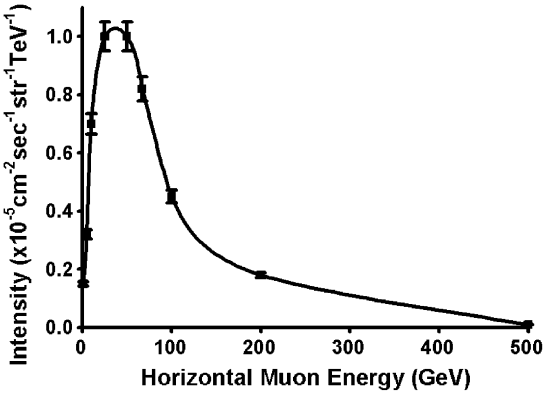

Fig. 1. The energy distribution of horizontal cosmic-ray muons.

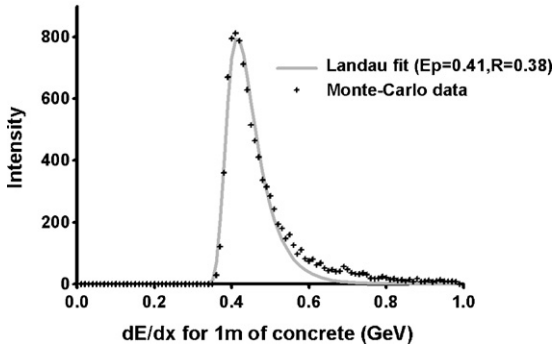

Fig. 3. The energy-loss distribution for a 50 GeV muon traversing 1 m of concrete, fitted to a Landau distribution with $E_p = 0.41$ and $R = 0.38$.

see Eq. (2).

$$\left.\frac{dE}{dx}\right]_{\text{Ionisation}} = 2\pi r_e^2 mc^2 n_{el}\frac{(z_p)^2}{\beta^2}\left[\ln\left(\frac{2mc^2\beta^2\gamma^2 T_{up}}{I^2}\right) - \beta^2\left(1+\frac{T_{up}}{T_{max}}\right) - \delta - \frac{2C_e}{Z}\right] \quad (2)$$

where r_e is the electron radius, mc^2 the rest mass energy of the electron, z_p the charge on the ion, n_{el} and Z the electron density and atomic number of the absorber, I the mean ionisation energy in the material, $\beta^2 = 1 - 1/(1+\gamma)^2$, $\gamma = T/mc^2$, T the kinetic energy of the ion, $T_{up} = \min(T_{cut}, T_{max})$, δ a density correction and C_e is a shell correction function (see GEANT4 documentation [5]).

For high-energy charged-particles of mass, m, the ionisation loss is at a minimum where $E \sim 3mc^2$. Below this energy, the ionisation cross-section rapidly increases. Particles with energies close to this minimum are often referred to as "minimum ionising particles". The ionisation cross-section (and hence energy deposited in a detector) then slowly increases again due to a relativistic rise in the stopping power, which is partially cancelled by the effect of density, see Fig. 2.

Minimum ionising particles are particles which travel through a medium with a minimum loss of ionisation energy. The energy deposited by muons in this region is approximately constant and the resulting average energy-loss spectrum is expected to show a narrow distribution. But since the energy-loss process is a statistical phenomenon, there are fluctuations in the energy lost by a charged-particle in thin layers (i.e. in a sample/detector whose thickness is much smaller than the range of the ion, e.g. 50 GeV muons have a mean range of 45 m in concrete). Such energy losses have been theoretically described by Landau [6], and it is the Landau expression, shown in Eq. (3), which shows the amount of ionisation liberated in a relatively thin absorber.

$$f(E) = \sqrt{\frac{e^{-(\lambda+e^{-\lambda})}}{2\pi}} \quad (3)$$

Here, λ is $R(E - E_p)$, E_p the most probable energy loss and R is a constant dependent on absorber. The energy-loss distribution is characterised by a narrow peak followed by a long tail towards a maximum value (due to smaller numbers of individual collisions, each with a small probability of transferring comparatively large amounts of energy). Fig. 3 shows the Landau distribution fitted to the energy loss of a 50 GeV muon traversing 1 m of concrete for 10,000 simulated muon events.

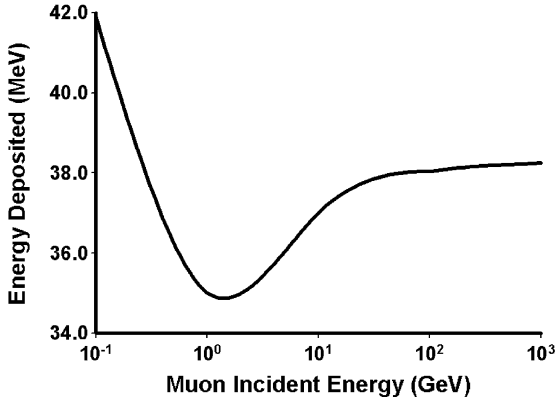

Fig. 2. The energy deposited in a 76.2 mm × 76.2 mm NaI(Tl) for muons with typical cosmic-ray energies.

3. Imaging methodologies

In attenuation loss techniques, the expected flux (from a measurement when there is no sample between the detectors) is compared to the measured number of four-fold coincident measurements (see geometrical arrangement of detectors in Fig. 4). This is of course reliant on a stable intensity of horizontal muons. Unfortunately, the naturally occurring flux varies with changes in atmospheric pressure. The advantage is that smaller cheaper detectors can be used as simple energy thresholded counters. Alternatively, energy-loss techniques would measure the energy of the muons before and after the sample. For 50 GeV muons, which of course have a long range in materials, the energy deposited in a detector, although large (typically >6.8 MeV g^{-1} cm^2), will vary only slightly as the reduction in energy for a 50 GeV is less than 1 GeV for 1 m thick samples. This change can be maximised by using larger detector volumes and higher Z detector materials.

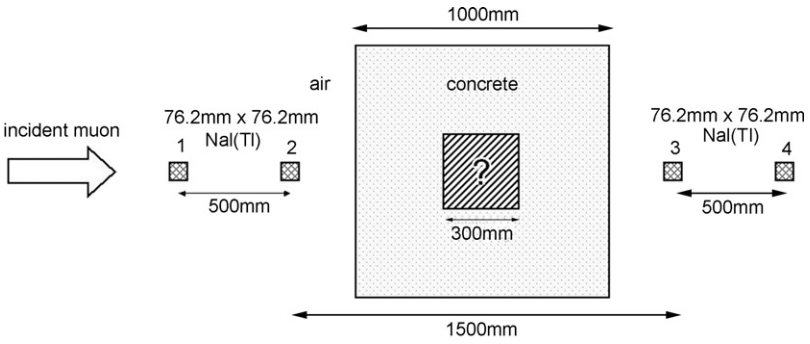

Fig. 4. Geometry used to compare the components of a four-fold telescope against energy-loss measurements for the identification of materials.

4. Monte-Carlo simulations

The geometry shown in Fig. 4 was used to compare the use of energy-loss techniques versus attenuation loss techniques using the GEANT4 radiation transportation Monte-Carlo code [5].

The muons were transported through the geometry so that they arrive centrally on the face of detector 1 and perpendicular to this face. The energy of the initial muon was taken to be 50 GeV to represent the mean energy of horizontal muons. Each material that was to be tested was positioned in a 30 cm cube in the centre of a 1 m cube of concrete as well as a calibration measurement with no sample between the detectors. The test materials were concrete, air, iron, lead and uranium. Ten thousands muons were started for each material and measurements of the change in the energy of the muon across the sample were compared to the attenuation (by scatter or capture) losses in the four-fold coincident measurements, see Table 1.

It should be noted that the horizontal flux of 10,000 muons used in the simulation would, under real experimental conditions using the naturally occurring flux of muons, take approximately 14 years, and it should also be noted that only higher Z elements show any appreciable intensity losses. The energy losses, though, allow material discrimination with only a handful of counts, see Fig. 5, as the differences in deposited energy are so great. This implies that if the energy of the muon before and after the sample can be measured the times needed per ray-sum will fall to a few days.

Table 1
Comparison of Monte-Carlo results for attenuation loss measurement and energy-loss measurements

Sample	Four-fold coincidences (for 10,000 incident muons)	Mean dE/dx (GeV)
No sample (just air)	9985	0.0003
Air cavity	9984	0.294
All concrete	9986	0.478
Embedded iron	9975	0.865
Embedded lead	9971	1.171
Embedded uranium	9955	2.232

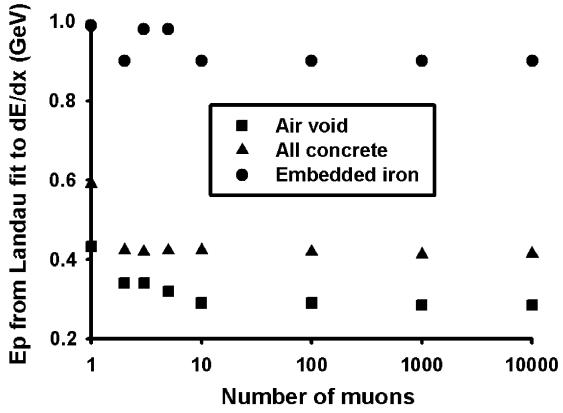

Fig. 5. Fit of dE/dx through different samples to a Landau distribution to determine the most probable energy vs. number of muons used to produce dE/dx distribution.

5. Conclusions

The use of muon energy-loss techniques in imaging of large vessels is a promising technique. The use of these highly penetrating but energetic particles means large objects can be studied and large energies are also deposited in any detector systems chosen [7]. It has been shown that the use of simple attenuation of horizontal muons takes years to accumulate enough statistics to see differences in samples which are easily discernable with muon energy-loss techniques using just a few muons. It should be noted that the muon energy employed, in this initial study, is the mean energy and the difficulty of the problem will be compounded with the naturally occurring horizontal muon energy distribution. It is also worth mentioning that the measurement of the muon energy before and after transmission through an object is not trivial. The detector resolution has to be such that the energy deposited in the detector by the initial energy of the muon should be sufficiently different to the energy deposited in the detector by the exiting muon.

Acknowledgement

We are grateful to British Nuclear Fuels plc for funding this research.

References

[1] P.M. Jenneson, Nucl. Instrum. Methods A 525 (2004) 346–351.
[2] T. Gaisser, Cosmic Rays and Particle Physics, Cambridge University Press, 1990, pp. 71-77.

[3] K. Nagamine, M. Iwasaki, K. Shimomura, K. Ishida, Nucl. Instrum. Methods A 356 (1995) 585–595.
[4] K. Haiwara, et al., Phys. Rev. D 66 (2002) 010001.
[5] S. Agostinelli, et al., Nucl. Instrum. Methods A 506 (2003) 250–303.
[6] L. Landau, J. Phys. USSR 8 (1944) 201.
[7] E.J. Morton And, S.J.R. Simons, The physical basis of process tomography, in: D.M. Scott, R.A. Williams (Eds.), Frontiers in Industrial Process Tomography, Engineering Foundation, New York, 1998, pp. 11–21.